Electric Power Systems Research 168 (2019) 336–349

Contents lists available at ScienceDirect

Electric Power Systems Research

journal homepage: www.elsevier.com/locate/epsr

Overall performance evaluation of reactive power control strategies in low voltage grids with high prosumer share

D.-L. Schultis*, A. Ilo, C. Schirmer

TU Wien, Institute of Energy Systems and Electrical Drives, Gußhausstraße 25/370-1, A-1040 Vienna, Austria

ARTICLE INFO

Keywords:
Distributed generation
Low voltage grid
Power factor correction
Volt/var control
Photovoltaic
Inverter

ABSTRACT

This paper presents an overall evaluation of different reactive power control strategies in low voltage grids with high prosumer share by means of social and technical criteria. Two types of control-devices, which fundamentally differ in their ownership structure, are considered: prosumer-owned photovoltaic-inverters and distribution system operator-owned inductive devices. Local cos$\varphi(P)$- and $Q(U)$-control of photovoltaic-inverters and local $L(U)$-control of inductive devices are separately simulated in various low voltage grids with radial structure and different cable share. $L(U)$-control is calculated also in presence of Q-Autarkic prosumers. Results show that the use of prosumer-owned PV-inverters to eliminate voltage violations on the feeder entails social and technical disadvantages such as prosumer discrimination, threat to their data privacy, high reactive power exchanges between low and medium voltage grid, high distribution transformer loading and high grid loss. In rural networks with relative long feeders and high PV-penetrations, the use of local controls of prosumer-owned inverters is not sufficient to eliminate all violations of the upper voltage limit. The application of inductive devices for voltage control does not entail social issues and enables a satisfactory technical performance of low voltage grids. The combination of $L(U)$-control and Q-Autarkic prosumers further improves the grid performance. Results show that the cos$\varphi(P)$-control strategy has the worst overall performance, while $L(U)$-control combined with Q-Autarkic prosumers has the best one.

1. Introduction

The increase of rooftop photovoltaic (PV) penetration in low voltage grids (LVG) challenges the traditional power system operation. In many cases, the reverse active power flow provoked by the dispersed PV-injections causes violations of the upper voltage limit [1]. European distribution system operators (DSO) have to ensure the compliance of their grid voltages with the EN 50160 limits of ± 10% around nominal voltage.

In power systems, OLTC transformers [1–3] and reactive power devices are usually used to control the voltage. In radial distribution grids, the use of OLTC transformers shifts the voltage profiles of all thereto connected feeders in parallel. In case of a large voltage spreading between the different feeders, this method may provoke new voltage violations. Capacitor banks are widely used to alleviate the violations of the lower voltage limit. To mitigate the violations of the upper voltage limit, other measures are discussed in literature such as: conventional grid reinforcement [1], var-control of inductive devices [3–5], var- and watt-control of PV-inverters [1–3], demand response [1] and storage operation [1]. While the first two measures are applied by the DSO, the latter ones are mainly provided by prosumers.

The most popular measures to mitigate the voltage limit violations are cos$\varphi(P)$- and $Q(U)$-local control of inverters that involve prosumer-owned devices in voltage control. Both control strategies mitigate the voltage violations by absorbing reactive power. A cos$\varphi(P)$-controlled PV-inverter absorbs reactive power beginning from a predefined active power injection. As well known, this control strategy has a strong voltage regulation ability [6] but does not consider the actual grid-voltage. Consequently, it provokes unnecessary large Q-flows and losses especially during high load and high production periods [6,7]. This disadvantage is improved by the $Q(U)$-control, which reduces the Q-flows and decreases the additional grid losses [8], but in return, it divides the reactive power compensation duty inequitably between the involved prosumers [9]. The latter provokes a new social issue, the customer discrimination in ancillary services provision.

Generally, uncoordinated local Q-controls provoke uncontrolled reactive power flows in the superordinate grids [10]. This disadvantage is well known and, in many cases, traditional Volt/var management technologies are used by utilities to coordinate the distribution transformer (DTR) step settings and the reactive power devices [11]. To

* Corresponding author.
E-mail address: daniel-leon.schultis@tuwien.ac.at (D.-L. Schultis).

https://doi.org/10.1016/j.epsr.2018.12.015
Received 28 March 2018; Received in revised form 10 December 2018; Accepted 12 December 2018

realize this coordination in low voltage level, an extensive data exchange between the prosumers and DSO is necessary that jeopardizes the strict data privacy requirements. To meet these data privacy requirements, Ref. [5] proposes to use locally controlled inductive devices set at the end of the violated low voltage feeders ($L(U)$-control). Ref. [4] goes further and proposes a Volt/var-control strategy ensemble, where the $L(U)$-control is combined with a Q-Autarky of prosumers. The latter uses the PV-inverter of each prosumer for a local power factor correction of the customer plant.

As discussed above, by attempting to reach a technical solution, new social issues are provoked that make their implementation in large scale almost impossible. Therefore, a common evaluation of the technical and social impacts of different solutions is required to identify the applicable ones.

This paper presents an overall evaluation of various reactive power control strategies in LVGs with high PV-penetration. For the first time are compared the well-known local $Q(U)$- and $\cos\varphi(P)$-control of PV-inverters together with the new $L(U)$-control strategy and its combination with Q-Autarkic prosumers by means of technical and social criteria. At the beginning, the test-system description is given that includes the sketch of LVGs, prosumer modelling and the description of the considered control strategies. Afterwards, the simulated scenarios are defined. The technical and social evaluation criteria are crucial for this study and therefore they are carefully specified. The simulation results and afterwards the overall performance evaluation of different control strategies are presented and visualized in different diagrams and charts. Finally, the conclusions are given.

2. Test systems description

The scope of this study is the LVG and the impact of the thereto connected customer plants on their behaviour. A short description of the test LVGs, the prosumers and the considered control strategies is given in the following.

2.1. Low voltage grids

Two types of LVGs are considered: theoretical and real ones. The included DTRs have a fixed tap set in middle position. The exact data of the considered test grids is given in [12].

2.1.1. Theoretical grids

Fig. 1 shows a schematic presentation of the theoretical LVGs. The same topology is used for both grids that consists of one main feeder with a length of 1 km and a 20 kV/0.4 kV, 160 kVA DTR. The feeder has cable or overhead line structure, Fig. 1(a) and (b), respectively. Two residential prosumers are connected equidistantly at each node through 10 m lines, resulting in totally 20 connected prosumers.

2.1.2. Real grids

Fig. 2 shows a schematic presentation of the considered real LVGs. Fig. 2(a) shows a typical urban LVG with nine main feeders. The longest

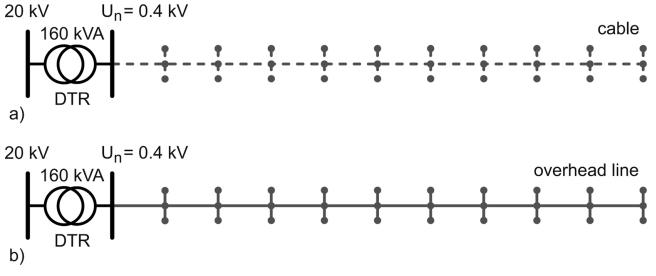

Fig. 1. Schematic presentation of different theoretical low voltage grids: (a) cable; (b) overhead line.

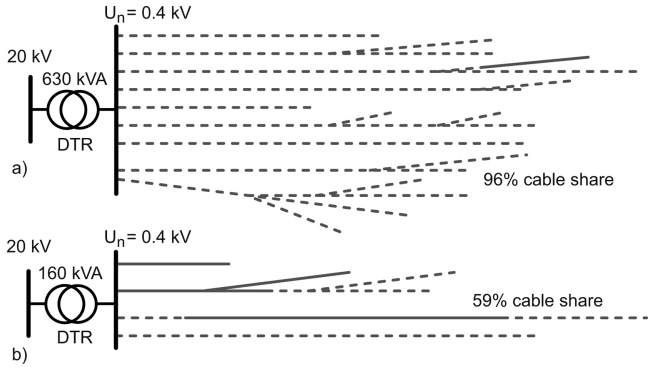

Fig. 2. Schematic presentation of different real low voltage grids: (a) urban; (b) rural.

of them is 1.27 km, while the shortest is 0.305 km long. In this grid with a 96% cable share are connected 175 residential prosumers. It is connected to the medium voltage grid (MVG) through a 20 kV/0.4 kV, 630 kVA DTR. Fig. 2(b) shows a typical rural LVG with four main feeders. The longest of them is 1.63 km, while the shortest is 0.565 km long. In this grid with a 59% cable share are connected 61 residential prosumers. It is connected to the MVG through a 20 kV/0.4 kV, 160 kVA DTR.

2.2. Prosumer modelling

Fig. 3 shows the used prosumer structure. It is characterized by the active and reactive power consumption and production of the internal loads (P_i^{load} and Q_i^{load}) and PV-systems (P_i^{inv} and Q_i^{inv}). Each prosumer i is connected to a grid-node with a voltage of U_i^{grid}. Voltage dependency of loads is modelled according to Eq. (1) with ZIP-coefficients for residential loads from [13], Table 1.

$$P_i^{\text{load}} = P_{\text{init}}^{\text{load}} \cdot \left(Z_P \cdot \left(\frac{U_i^{\text{grid}}}{U_n} \right)^2 + I_P \cdot \frac{U_i^{\text{grid}}}{U_n} + P_P \right) \tag{1}$$

where:

$P_{\text{init}}^{\text{load}}$ – initial value of the active power consumption of each prosumer;

$U_n = 0.4$ kV – nominal voltage of LVG;

Z_P, I_P, P_P – ZIP-coefficients for active power consumption.

The same formula is used to express the voltage dependency of the reactive part of the load (Q_i^{load}). An initial power factor of 0.95 is set for all loads, so that $Q_{\text{init}}^{\text{load}} = P_{\text{init}}^{\text{load}} \cdot \tan(\arccos(0.95))$. The PV-system of each prosumer contains PV-modules with a rating of $P_r^{\text{PV}} = 5$ kW and an inverter with a rating of $S_r^{\text{inv}} = P_r^{\text{PV}}/0.9$. The reactive power production of each inverter is determined by the applied control strategy (see

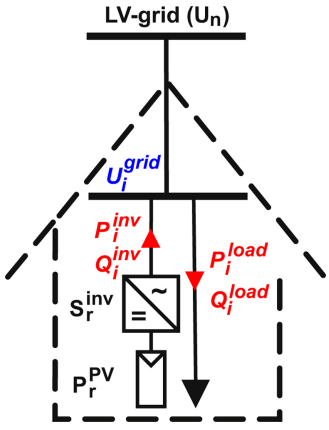

Fig. 3. Structure of a prosumer.

Table 1
Load ZIP coefficients.

Z_P	I_P	P_P	Z_Q	I_Q	P_Q
0.96	−1.17	1.21	6.28	−10.16	4.88

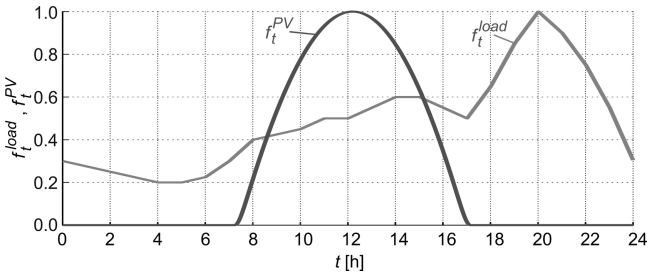

Fig. 4. Load and PV-production profile of all prosumers.

Section 2.3). If no inverter control is applied, PV-systems inject with power factor one. Losses within PV-systems are neglected in all simulations. Fig. 4 shows the load (f_t^{load}) and PV-production (f_t^{PV}) profile of all prosumers.

2.3. Local control strategies

In the evaluation process are considered the two most popular local control strategies, cos$\varphi(P)$- and $Q(U)$-control, and two new ones, $L(U)$-control and its combination with Q-Autarkic prosumers.

2.3.1. cos$\varphi(P)$-control

Fig. 5 shows the cos$\varphi(P)$-characteristic which is suggested by the Austrian grid code [14] and used in this study. Based on that characteristic, the inverter of each prosumer i absorbs reactive power if its normalized active power production ($p_i^{\text{PV}} = P_i^{\text{inv}}/P_r^{\text{PV}}$) exceeds a value of 0.5.

2.3.2. Q(U)-control

Fig. 6 shows the fundamental $Q(U)$-characteristic suggested by the Austrian grid code [14]. The parameters u_a, u_b, u_c and u_d can be specified by the responsible DSO according to the prevalent grid conditions. The $Q(U)$-characteristics are set to eliminate voltage limit violations for maximal voltages and to avoid unnecessary reactive power flows within the LVG for admissible voltages. For each test-grid, one specific $Q(U)$-characteristic is used for all prosumers. Table 2 shows the corresponding parameters, i.e. u_a, u_b, u_c and u_d. The minimum requirements and a safety margin for the slope gradient are respected [2]. The adequacy of the parameter selection is given for both real grids in Appendix A, Figs. 29 and 30 .

2.3.3. L(U)-control

In this case, PV-inverters inject by power factor one, and prosumers draw reactive power from the LVG to supply their loads. Inductive

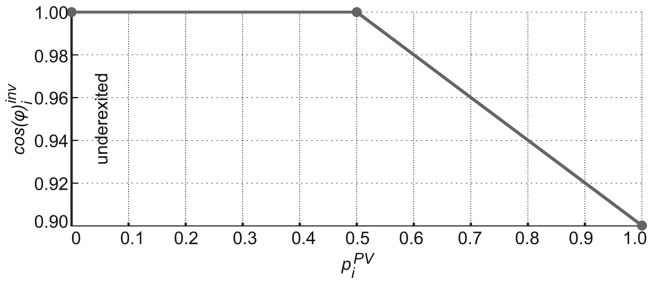

Fig. 5. cos$\varphi(P)$-characteristics suggested by the Austrian grid code.

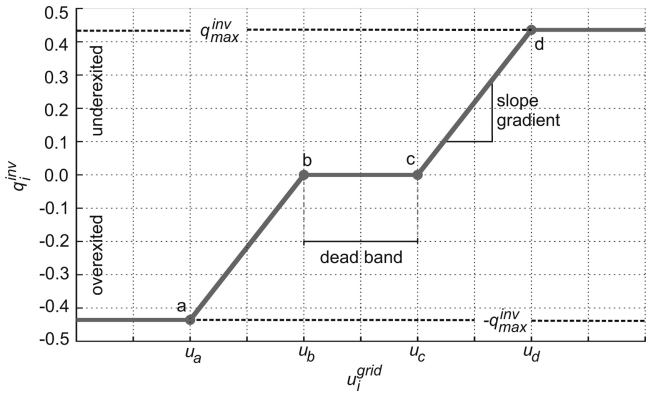

Fig. 6. Fundamental $Q(U)$-characteristic suggested by the Austrian grid code.

Table 2
$Q(U)$-parameterizations used for the different test-grids.

Test-grid	u_a [p.u.]	u_b [p.u.]	u_c [p.u.]	u_d [p.u.]
Urban	0.91	0.94	1.04	1.07
Rural	0.90	0.93	1.00	1.03
Cable	0.91	0.94	1.05	1.08
Overhead line	0.90	0.93	1.07	1.10

devices with continuous variable reactances are used to model the local $L(U)$-control. They are located at the end of each violated feeder [4]. $L(U)$-controls are activated only for local voltages larger than a predefined voltage, $U_{set-point}$. The inductive devices absorb the needed reactive power to prevent a local exceedance of $U_{set-point}$. Active power losses of inductive devices are neglected. $U_{set-point}$ is set to 1.09 p.u.. Fig. 7 shows a schematic LVG with two $L(U)$-controlled feeders; the inductive devices are realized as shunt-coils in this case.

2.3.4. L(U)-control combined with Q-Autarkic prosumers

This control ensemble uses the $L(U)$ local control to mitigate voltage limit violations in LVG, and simultaneously Q-Autarky of prosumers. Per definition, Q-Autarkic prosumers fully compensate the reactive power needs in customer plant level ($Q_i^{\text{inv}} = Q_i^{\text{load}}$) at all times, acting reactive power self-sufficient [4]. Consequently, Q-Autarkic prosumers do not exchange any reactive power with the LVG.

3. Scenario definition

Various scenarios are considered to analyze the impact of different control strategies on the behaviour of each test-grid. Load and production, DTR primary voltage and the applied control strategy are varied to specify the scenarios.

3.1. Load and production

The active power consumption and production of all prosumers is defined by the load- and production profiles shown in Fig. 4. The time horizon of 24 h is sampled into one minute time steps, resulting in 1440 load flow simulations per scenario. The initial load value and the PV-production of all prosumers are determined for each time step by Eqs.

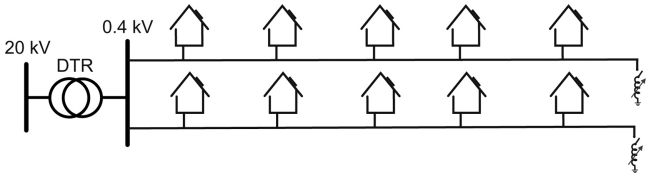

Fig. 7. Schematic LVG with two $L(U)$-controlled feeders.

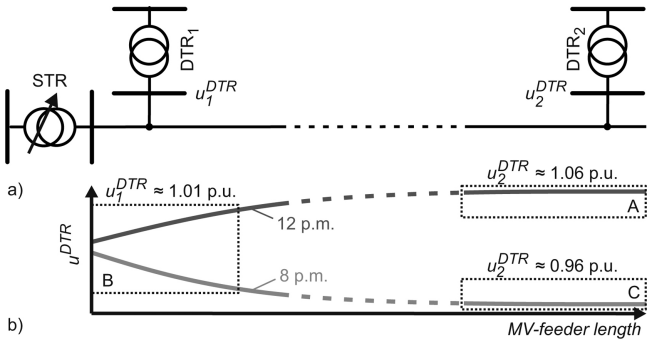

Fig. 8. Correlation of MVG voltage behaviour and DTR primary voltage: (a) schematic MV-feeder; (b) corresponding voltage profile for 12 p.m. and 8 p.m.

(2) and (3), respectively.

$$P_{\text{init},t}^{\text{load}} = f_t^{\text{load}} \cdot \widehat{P}^{\text{load}} \tag{2}$$

where:

$P_{\text{init},t}^{\text{load}}$ – initial active power consumption value of each prosumer at time step t;

f_t^{load} – load factor of each prosumer at time step t according to Fig. 4;

$\widehat{P}^{\text{load}} = 1.96$ kW – for the urban grid;

$\widehat{P}^{\text{load}} = 1.37$ kW – for the rural and both theoretical grids.

$$P_{i,t}^{\text{inv}} = f_t^{\text{PV}} \cdot P_r^{\text{PV}} \tag{3}$$

where:

$P_{i,t}^{\text{inv}}$ - active power injection of the inverter of prosumer i at time step t

f_t^{PV} – PV-production factor of each prosumer at time step t according to Fig. 4.

3.2. DTR primary voltage

DTRs have fixed tap-positions, thus the voltage variations at their primary sides are directly transmitted to the secondary ones. Fig. 8(a) shows a schematic MV-feeder with two connected DTRs, one close to the supplying transformer (STR), and the other at the end of the MV-feeder. Fig. 8b) shows the corresponding voltage profile for midday, 12 p.m., and for evening, 8 p.m.. The voltage profile of the MV-feeder changes significantly during a sunny day: At midday, the MV-feeder voltage increases because of the PV-production, while in the evening, it decreases because of the load consumption. Three areas A, B and C with three distinct voltages around 1.06, 1.01 and 0.96 p.u., respectively, are identified and marked in Fig. 8(b). For simplicity, the MVG is not included in the simulations, but its voltage variations during the day are considered in different scenarios by setting the DTR primary voltage to the three voltage values mentioned above.

3.3. Control strategies

The simulations are conducted for no-control and for all control strategies described in Section 2.3, i.e. cos$\varphi(P)$-, $Q(U)$-, $L(U)$- and $L(U)$-control combined with Q-Autarkic prosumers.

3.4. Scenario overview

Table 3 shows an overview of the simulated scenarios. They are applied to each test-grid. No-control and all control strategies mentioned in Section 3.3 are simulated separately for each DTR primary voltage by considering the load- and production-profile shown in Fig. 4.

Table 3
Overview of the simulated scenarios.

	Simulated scenarios		
u^{DTR}	1.06 p.u.	1.01 p.u.	0.96 p.u.
Control strategies	No-control cos$\varphi(P)$ $Q(U)$ $L(U)$ $L(U)$ and Q-Autarky	No-control cos$\varphi(P)$ $Q(U)$ $L(U)$ $L(U)$ and Q-Autarky	No-control cos$\varphi(P)$ $Q(U)$ $L(U)$ $L(U)$ and Q-Autarky

4. Evaluation process

The effectiveness and applicability of the different solutions is assessed by means of technical and social evaluation criteria.

4.1. Evaluation criteria

The technical and social evaluation criteria are described in Sections 4.1.1 and 4.1.2.

4.1.1. Technical criteria

The main effect of each Volt/var local control strategy, i.e. the impact on grid-voltage, is associated with side effects, i.e. the additional reactive power exchange between MVG and LVG, DTR loading and grid loss. Therefore, the technical criteria are divided into primary and secondary criteria representing the main and side effects, respectively.

Average voltage violation index – The main effect of the considered control strategies is the mitigation of voltage limit violations in LVG. Its impact is assessed by the average voltage violation index (primary criterion). The voltage violation index, and its peak and average value are calculated according to Eqs. (4)–(6).

$$\text{VI}_t = \frac{\sum_{j=1}^{m_t} (U_{j,t}^{\text{viol}} - U_{\text{lim}}^{\text{upper}})}{U_n} + \frac{\sum_{j=1}^{n_t} (U_{\text{lim}}^{\text{lower}} - U_{j,t}^{\text{viol}})}{U_n} \tag{4}$$

where:

VI_t – voltage violation index for time step t;

m_t – number of grid-nodes that violate the upper limit at time step t;

n_t – number of grid-nodes that violate the lower limit at time step t;

$U_{j,t}^{\text{viol}}$ – voltage value of violated grid-node j at time step t;

$U_{\text{lim}}^{\text{upper}} = 0.44$ kV – upper voltage limit;

$U_{\text{lim}}^{\text{lower}} = 0.36$ kV – lower voltage limit.

$$\widehat{\text{VI}} = \max_t(\text{VI}_t) \tag{5}$$

where:

$\widehat{\text{VI}}$ – peak voltage violation index.

$$\overline{\text{VI}} = \frac{1}{1440} \cdot \sum_{t=1}^{1440} \text{VI}_t \tag{6}$$

where:

$\overline{\text{VI}}$ – average voltage violation index;

1440 – number of load flow simulations per scenario.

Reactive energy exchange – One of the side effects of the considered control strategies is the additional uncontrolled Q-exchange between the MVG and LVG. Its impact is assessed by the reactive energy exchanged over the simulated time horizon of 24 h (secondary criterion). The peak Q-exchange and the reactive energy exchange are calculated according to Eqs. (7) and (8), respectively.

$$\widehat{Q}^{\text{ex}} = \max_t(Q_t^{\text{ex}}) \tag{7}$$

where:

Q_t^{ex} – Q-exchange at primary side of DTR for time step t;

$\widehat{Q}^{\text{ex}}$ – peak Q-exchange.

$$E^{Q_{ex}} = \frac{1}{60} h \cdot \sum_{t=1}^{1440} Q_t^{ex} \tag{8}$$

where:

$E^{Q_{ex}}$ – reactive energy exchange between MVG and LVG.

Average DTR loading – Another side effect of the considered control strategies is the increase of DTR loading. Its impact is assessed by the average DTR loading (secondary criterion). The peak and average DTR loading are calculated according to Eqs. (9) and (10), respectively.

$$\widehat{\overline{\mathrm{DTRL}}} = \max_t(\mathrm{DTRL}_t) \tag{9}$$

where:

$DTRL_t$ – DTR loading for time step t;

$\widehat{\overline{\mathrm{DTRL}}}$ – peak DTR loading.

$$\overline{\mathrm{DTRL}} = \frac{1}{1440} \cdot \Sigma_{t=1}^{1440} \mathrm{DTRL}_t \tag{10}$$

where:

$\overline{\mathrm{DTRL}}$ – average DTR loading.

Energy loss – The third side effect of the considered control strategies is the additional active power loss of feeders and DTR. Its impact is assessed by the energy loss over the simulated time horizon of 24 h (secondary criterion). The peak and energy loss are calculated according to Eqs. (11) and (12), respectively.

$$\widehat{P}^{\mathrm{loss}} = \max_t(P_t^{\mathrm{loss}}) \tag{11}$$

where:

P_t^{loss} – active power loss of feeders and DTR at time step t;

$\widehat{P}^{\mathrm{loss}}$ – peak active power loss of feeders and DTR.

$$E^{P_{\mathrm{loss}}} = \frac{1}{60} h \cdot \sum_{t=1}^{1440} P_t^{\mathrm{loss}} \tag{12}$$

where:

$E^{P_{\mathrm{loss}}}$ – energy loss of feeders and DTR.

To realize an overall performance evaluation of the considered control strategies, all simulation results are concisely presented in a spider chart. The spider chart data are calculated as follows. Firstly, the results of each criterion ($\overline{\mathrm{VI}}$, $E^{Q_{ex}}$, $E^{P_{\mathrm{loss}}}$ and $\overline{\mathrm{DTRL}}$) are superposed for all three DTR primary voltages according to Eqs. (13)–(16):

$$\overline{\mathrm{VI}}_{g,c} = \sum_{\forall v} \overline{\mathrm{VI}}_{g,c,v} \tag{13}$$

where:

$\overline{\mathrm{VI}}_{g,c,v}$ – average voltage violation index for test-grid g, control strategy c and DTR primary voltage v;

$\overline{\mathrm{VI}}_{g,c}$ – aggregated average voltage violation index for test-grid g and control strategy c.

$$E_{g,c}^{Q_{ex}} = \sum_{\forall v} E_{g,c,v}^{Q_{ex}} \tag{14}$$

where:

$E_{g,c,v}^{Q_{ex}}$ – reactive energy exchange for test-grid g, control strategy c and DTR primary voltage v;

$E_{g,c}^{Q_{ex}}$ – aggregated reactive energy exchange for test-grid g and control strategy c.

$$\overline{\mathrm{DTRL}}_{g,c} = \sum_{\forall v} \overline{\mathrm{DTRL}}_{g,c,v} \tag{15}$$

where:

$\overline{\mathrm{DTRL}}_{g,c,v}$ – average DTR loading for test-grid g, control strategy c and DTR primary voltage v;

$\overline{\mathrm{DTRL}}_{g,c}$ – aggregated average DTR loading for test-grid g and control strategy c.

$$E_{g,c}^{P_{\mathrm{loss}}} = \sum_{\forall v} E_{g,c,v}^{P_{\mathrm{loss}}} \tag{16}$$

where:

$E_{g,c,v}^{P_{\mathrm{loss}}}$ – active energy loss for test-grid g, control strategy c and DTR primary voltage v;

$E_{g,c}^{P_{\mathrm{loss}}}$ – aggregated active energy loss for test-grid g and control strategy c.

Secondly, the resulting values are normalized according to Eqs. (17)–(20):

$$\overline{\mathrm{vi}}_{g,c} = \frac{\overline{\mathrm{VI}}_{g,c}}{\max_c(\overline{\mathrm{VI}}_{g,c})} \tag{17}$$

where:

$\overline{\mathrm{vi}}_{g,c}$ – normalized aggregated average voltage violation index for test-grid g and control strategy c.

$$e_{g,c}^{Q_{ex}} = \frac{E_{g,c}^{Q_{ex}}}{\max_c(E_{g,c}^{Q_{ex}})} \tag{18}$$

where:

$e_{g,c}^{Q_{ex}}$ – normalized aggregated reactive energy exchange for test-grid g and control strategy c.

$$\overline{\mathrm{dtrl}}_{g,c} = \frac{\overline{\mathrm{DTRL}}_{g,c}}{\max_c(\overline{\mathrm{DTRL}}_{g,c})} \tag{19}$$

where:

$\overline{\mathrm{dtrl}}_{g,c}$ – normalized aggregated average DTR loading for test-grid g and control strategy c.

$$e_{g,c}^{P_{\mathrm{loss}}} = \frac{E_{g,c}^{P_{\mathrm{loss}}}}{\max_c(E_{g,c}^{P_{\mathrm{loss}}})} \tag{20}$$

where:

$e_{g,c}^{P_{\mathrm{loss}}}$ – normalized aggregated active energy loss for test-grid g and control strategy c.

Finally, the resulting values for both real LVGs are merged according to Eqs. (21)–(24):

$$\overline{\mathrm{vi}}_c = \frac{\overline{\mathrm{vi}}_{g=u,c} + \overline{\mathrm{vi}}_{g=r,c}}{2} \tag{21}$$

where:

$\overline{\mathrm{vi}}_{g=u,c}$ – normalized aggregated average voltage violation index for the urban grid and control strategy c;

$\overline{\mathrm{vi}}_{g=r,c}$ – normalized aggregated average voltage violation index for the rural grid and control strategy c;

$\overline{\mathrm{vi}}_c$ – normalized aggregated average voltage violation index for both real grids and control strategy c.

$$e_c^{Q_{ex}} = \frac{e_{g=u,c}^{Q_{ex}} + e_{g=r,c}^{Q_{ex}}}{2} \tag{22}$$

where:

$e_{g=u,c}^{Q_{ex}}$ – normalized aggregated reactive energy exchange for the urban grid and control strategy c;

$e_{g=r,c}^{Q_{ex}}$ – normalized aggregated reactive energy exchange for the rural grid and control strategy c;

$e_c^{Q_{ex}}$ – normalized aggregated reactive energy exchange for both real grids and control strategy c.

$$\overline{\mathrm{dtrl}}_c = \frac{\overline{\mathrm{dtrl}}_{g=u,c} + \overline{\mathrm{dtrl}}_{g=r,c}}{2} \tag{23}$$

where:

$\overline{\mathrm{dtrl}}_{g=u,c}$ – normalized aggregated average DTR loading for the urban grid and control strategy c;

$\overline{\mathrm{dtrl}}_{g=r,c}$ – normalized aggregated average DTR loading for the rural grid and control strategy c;

$\overline{\mathrm{dtrl}}_c$ – normalized aggregated average DTR loading for both real grids and control strategy c.

$$e_c^{P_{\text{loss}}} = \frac{e_{g=u,c}^{P_{\text{loss}}} + e_{g=r,c}^{P_{\text{loss}}}}{2} \tag{24}$$

where:

$e_{g=1,c}^{P_{\text{loss}}}$ – normalized aggregated energy loss for the urban grid and control strategy c;

$e_{g=2,c}^{P_{\text{loss}}}$ – normalized aggregated energy loss for the rural grid and control strategy c;

$e_c^{P_{\text{loss}}}$ – normalized aggregated energy loss for both real grids and control strategy c.

As a result, the normalized values lie in between 0 and 1 and can be properly presented in the spider chart.

4.1.2. Social criteria

Discrimination – In general, the aim of a non-discrimination law is to allow all individuals an equal and fair prospect to access opportunities available in a society. Regarding the operation of LVGs, an opportunity for prosumers is to support the grid operation by offering reactive power as an ancillary service. According to [15], the procurement of such ancillary services by DSOs shall be transparent, non-discriminatory and market-based, ensuring an effective participation of all market players. In a non-discriminatory market, the applied control strategy should enable all prosumers an equal and fair participation in ancillary service provision. The discrimination criterion is set to one or to zero, when discrimination is present or not, respectively.

Data privacy – A coordinated control approach requires data exchanges between the control devices, i.e. inverters and inductive devices, and a controller. To guarantee the data privacy of prosumers, the applied control strategy should allow a coordination of the underlying control devices without requiring any detailed data exchanges between prosumers and the DSO. The data privacy criterion is set to one or to zero, when privacy is violated or not, respectively.

4.2. Result visualisation

Fig. 9 shows the spider chart which is used to visualize the assessments of the Volt/var control strategies. On its corners are set all considered technical criteria described above. The overall performance of the different control strategies is characterized by the chart surface. The bigger its surface, the worse is the overall performance of the control strategy. The worst performance is indicated by a completely filled area and the ideal one corresponds to a point in the middle of the chart.

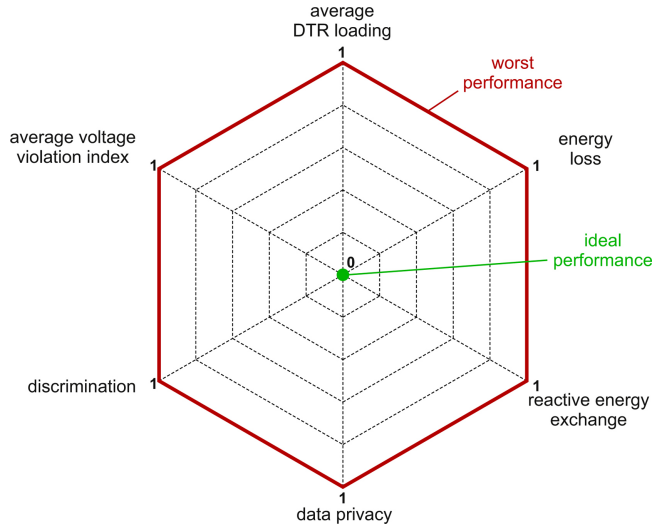

Fig. 9. Hexagon with the worst and ideal performance of the control strategies.

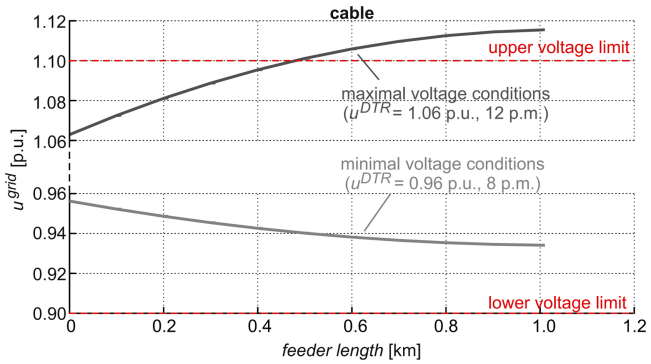

Fig. 10. Voltage profile of the theoretical cable grid with no-control for maximal and minimal voltage conditions.

5. Evaluation of *Q*-control strategies

The technical and social criteria are intensively discussed in Sections 5.1 and 5.2. Section 5.3 gives the overall evaluation of the different control strategies: for each theoretical grid separately, and for both real grids commonly.

5.1. Technical criteria

The technical criteria are apart evaluated for the theoretical and real LVGs. Although all scenarios defined in Section 3.4 are simulated, only the most relevant cases are discussed in this section. For each test-grid are discussed the primary criterion for maximal (u^{DTR} = 1.06 p.u., at 12 p.m.) and minimal (u^{DTR} = 0.96 p.u., at 8 p.m.) voltage conditions as well as the daily behaviour of the secondary criteria.

5.1.1. Theoretical grids

Theoretical cable grid – Fig. 10 shows the voltage profile of the cable grid with no-control for maximal and minimal voltage conditions. For maximal voltage conditions, the profile lies within and above the upper part of the allowed voltage range, resulting in a peak voltage violation index of 0.182. The calculation over the 24 h time horizon yields an average voltage violation index (primary criterion) of 0.020 for a DTR primary voltage of 1.06 p.u. For minimal voltage conditions, the profile stays within the lower part of the allowed voltage range throughout the whole day. Fig. 11 shows the voltage profile of the cable grid for maximal voltage conditions and different control strategies. All control strategies eliminate the violations of the upper voltage limit throughout the whole day. Fig. 12 shows the daily behaviour of the secondary criteria for the cable grid with no-control and with different control strategies for a DTR primary voltage of 1.06 p.u. The *Q*-exchange, DTR loading and loss are shown in Fig. 12(a)–(c), respectively. Simulation results show that cos$\varphi(P)$-control provokes the maximal peak *Q*-exchange and DTR loading of 50.17 kvar and 56.62%, respectively. Furthermore, $Q(U)$-control provokes the maximal reactive energy exchange, average DTR loading and energy loss as follows:

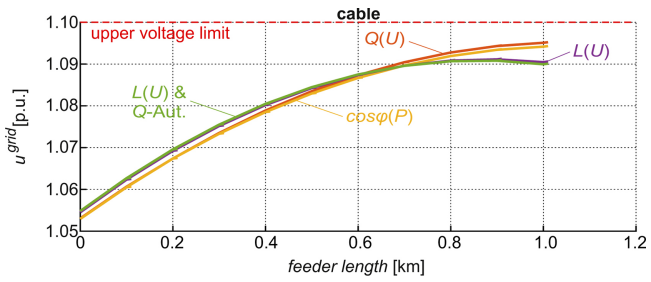

Fig. 11. Voltage profile of the theoretical cable grid for maximal voltage conditions and different control strategies.

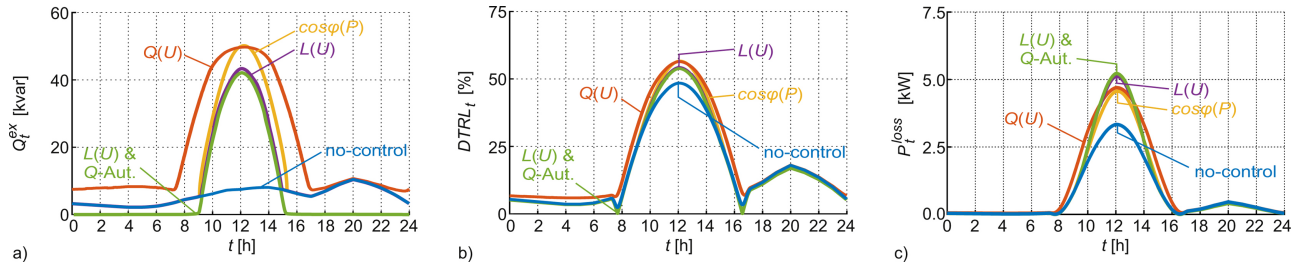

Fig. 12. Daily behaviour of the secondary criteria for the theoretical cable grid with no-control and with different control strategies for a maximum DTR primary voltage of 1.06 p.u.: (a) *Q*-exchange; (b) DTR loading; (c) active power loss.

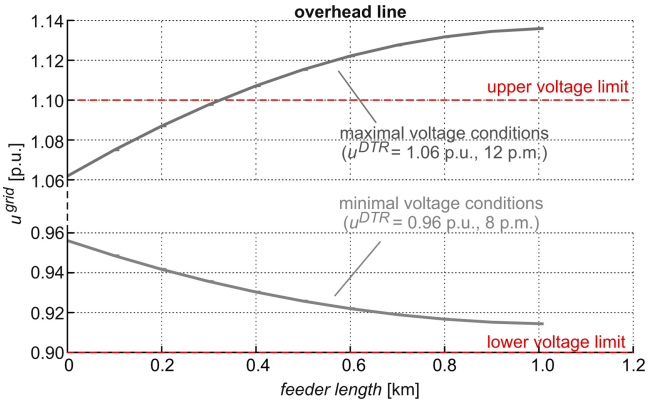

Fig. 13. Voltage profile of the theoretical overhead line grid with no-control for maximal and minimal voltage conditions.

$E^{Q_{ex}}$ = 470.22 kvarh, $\overline{\text{DTRL}}$ = 20.54% and $E^{P_{loss}}$ = 25.79 kWh. *L*(*U*)-control combined with *Q*-Autarkic prosumers provokes the maximal peak loss of 5.22 kW, the minimal *Q*-exchange in peak, 42.13 kvar, and in total, 169.16 kvarh, and the minimal DTR loading in peak, 53.84%, and on average, 17.46%. The minimal peak and energy loss of 4.57 kW and 21.90 kWh, respectively, is provoked by cos*φ*(*P*)-control.

Theoretical overhead line grid – Fig. 13 shows the voltage profile of the overhead line grid with no-control for maximal and minimal voltage conditions. For maximal voltage conditions, the profile lies within and above the upper part of the allowed voltage range, resulting in a peak voltage violation index of 0.526. The calculation over the 24 h time horizon yields an average voltage violation index (primary criterion) of 0.076 for a DTR primary voltage of 1.06 p.u. For minimal voltage conditions, the profile stays within the lower part of the allowed voltage range throughout the whole day. Fig. 14 shows the voltage profile of the overhead line grid for maximal voltage conditions and different control strategies. All control strategies eliminate the violations of the upper voltage limit throughout the whole day. Fig. 15 shows the daily behaviour of the secondary criteria for the overhead line grid with no-control and with different control strategies for a DTR primary voltage of 1.06 p.u.. The *Q*-exchange, DTR loading and loss are shown in

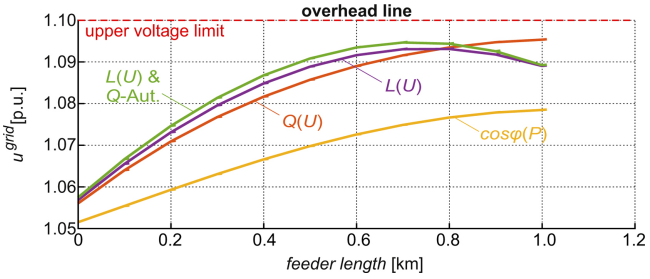

Fig. 14. Voltage profile of the theoretical overhead line grid for maximal voltage conditions and different control strategies.

Fig. 15(a)–(c), respectively. Simulation results show that cos*φ*(*P*)-control provokes the maximal values for all secondary criteria as follows: $\hat{Q}^{ex}$ = 55.55 kvar; $E^{Q_{ex}}$ = 341.09 kvarh; $\widehat{\text{DTRL}}$ = 57.29%; $\overline{\text{DTRL}}$ = 18.59 %; $\hat{P}^{loss}$ = 7.11 kW and $E^{P_{loss}}$ = 33.74 kWh. Meanwhile, *Q*(*U*)-control provokes the minimal peak loss of 6.09 kW. *L*(*U*)-control combined with *Q*-Autarkic prosumers provokes the minimal *Q*-exchange in peak, 30.37 kvar, and in total, 144.46 kvarh, the minimal DTR loading in peak, 50.31%, and on average, 16.97% and the minimal loss in peak, 6.11 kW, and in total, 29.83 kWh.

5.1.2. Real grids

Real urban grid – Fig. 16 shows the voltage profiles of all feeders of the urban grid with no-control for maximal and minimal voltage conditions. For maximal voltage conditions, all profiles lie within and above the upper part of the allowed voltage range; five feeders violate the upper voltage limit, resulting in a peak voltage violation index of 2.006. The calculation over the 24 h time horizon yields an average voltage violation index (primary criterion) of 0.260 for a DTR primary voltage of 1.06 p.u. For minimal voltage conditions, the profile stays within the lower part of the allowed voltage range throughout the whole day. Fig. 17 shows the voltage profiles of all feeders of the urban grid for maximal voltage conditions and different control strategies. They are shown for cos*φ*(*P*)-, *Q*(*U*)-, *L*(*U*)- and *L*(*U*)-control combined with *Q*-Autarkic prosumers in Figs. 17(a)–17 (d). All control strategies eliminate the violations of the upper voltage limit throughout the whole day.

Figs. 18–20 show the daily behaviour of the secondary criteria for the urban grid with no-control and with different control strategies for different DTR primary voltages of 1.06, 1.01 and 0.96 p.u., respectively. For all DTR primary voltages, if no-control is exercised, the *Q*-exchange is determined exclusively by the prosumers' consumption and thus follows the load profile shown in Fig. 4, while the DTR loading and grid loss are determined by their consumption and PV-production. Consequently, if no-control is exercised, the peak *Q*-exchange occurs at around 8 p.m. for all DTR primary voltages. Results show that *L*(*U*)-control, if combined with *Q*-Autarkic prosumers, and cos*φ*(*P*)-control, are active only during PV-production periods for all DTR primary voltages. For a maximum DTR primary voltage of 1.06 p.u., *Q*(*U*)-control is active throughout the whole day; for a medium DTR primary voltage of 1.01 p.u., it is active only during PV-production periods; and for a minimum DTR primary voltage of 0.96 p.u., it is active during PV-production and high load (at around 8 p.m.) periods. *L*(*U*)-control, if not combined with *Q*-Autarkic prosumers, is active only during PV-production periods for DTR primary voltages of 1.06 and 1.01 p.u., but for lower DTR primary voltages, e.g. 0.96 p.u., it is inactive throughout the whole day. cos*φ*(*P*)-, *Q*(*U*)- and *L*(*U*)-control combined with *Q*-Autarkic prosumers provoke the peak *Q*-exchange at around 12 p.m. for all DTR primary voltages. If *L*(*U*)-control is not combined with *Q*-Autarkic prosumers, it provokes the peak *Q*-exchange at around 12 p.m. for a DTR primary voltage of 1.06 p.u., and at around 8 p.m., for DTR primary voltages of 1.01 and 0.96 p.u., respectively.

Fig. 18 shows the daily behaviour of the secondary criteria for the

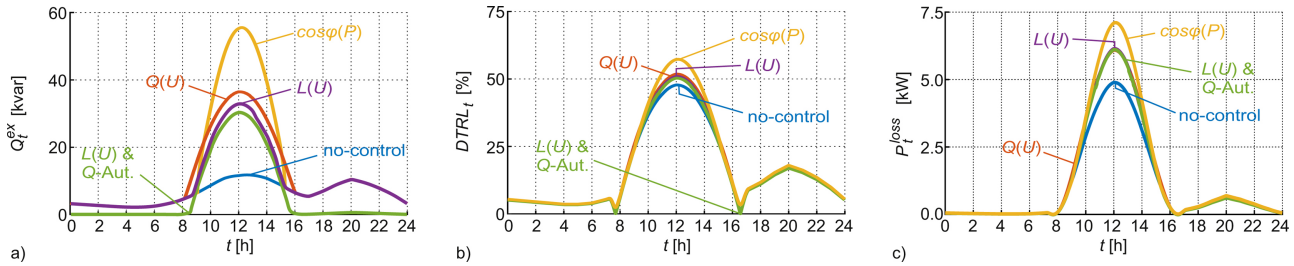

Fig. 15. Daily behaviour of the secondary criteria for the theoretical overhead line grid with no-control and with different control strategies for a maximum DTR primary voltage of 1.06 p.u.: (a) *Q*-exchange; (b) DTR loading; (c) active power loss.

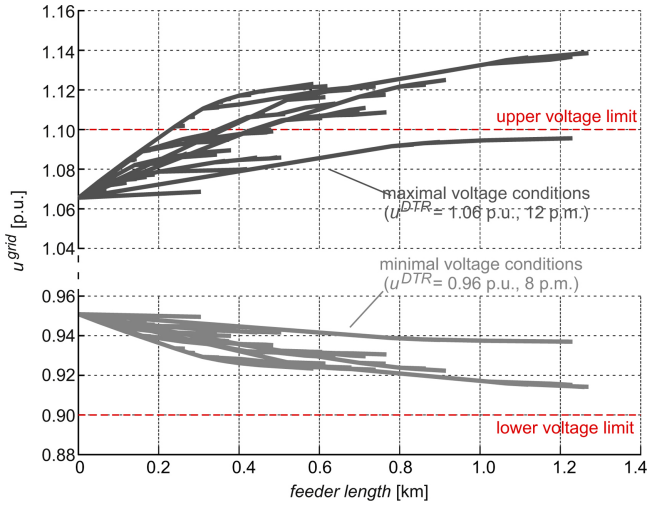

Fig. 16. Voltage profiles of all feeders of the urban grid with no-control for maximal and minimal voltage conditions.

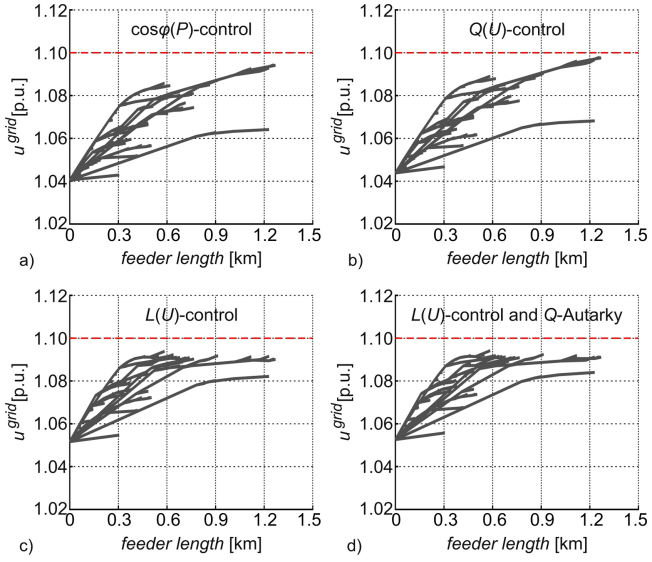

Fig. 17. Voltage profiles of all feeders of the urban grid for maximal voltage conditions and different control strategies: (a) cos*φ*(*P*); (b) *Q*(*U*); (c) *L*(*U*); (d) *L*(*U*) combined with *Q*-Autarkic prosumers.

urban grid with no-control and with different control strategies for a DTR primary voltage of 1.06 p.u. The *Q*-exchange is shown in Fig. 18(a); the DTR loading in Fig. 18(b) and the loss in Fig. 18(c). Simulation results show that cos*φ*(*P*)-control provokes the maximal peak values for all secondary criteria as follows: $\widehat{Q}^{ex}$ = 494.24 kvar; $\widehat{\text{DTRL}}$ = 130.13% and $\widehat{P}^{loss}$ = 49.90 kW. Meanwhile, *Q*(*U*)-control provokes the maximal reactive energy exchange and energy loss of 4762.96 kvarh and 275.66 kWh, respectively, and therefore also the maximal average DTR loading of 49.26%. The minimal peak loss of 47.33 kW is provoked by *L*(*U*)-control, while the minimal energy loss of 223.75 kWh is reached by its combination with *Q*-Autarkic prosumers. This combination also provokes the minimal *Q*-exchange in peak, 289.62 kvar, and in total, 1221.07 kvarh, and the minimal DTR loading in peak, 113.39%, and on average, 38.59%.

Fig. 19 shows the daily behaviour of the secondary criteria for the urban grid with no-control and with different control strategies for a DTR primary voltage of 1.01 p.u. The *Q*-exchange is shown in Fig. 19(a); the DTR loading in Fig. 19(b) and the loss in Fig. 19(c). Simulation results show that cos*φ*(*P*)-control provokes the maximal peak values for all secondary criteria as follows: $\widehat{Q}^{ex}$ = 487.28 kvar; $\widehat{\text{DTRL}}$ = 136.34% and $\widehat{P}^{loss}$ = 54.71 kW. Furthermore, it provokes the maximal reactive energy exchange and energy loss of 2976.37 kvarh and 259.92 kWh, respectively, and therefore also the maximal average DTR loading of 44.31%. The minimal peak and energy loss of 35.92 kW and 186.50 kWh, respectively, is provoked by *L*(*U*)-control combined with *Q*-Autarkic prosumers. This combination also provokes the minimal *Q*-exchange in peak, 24.64 kvar, and in total, 67.59 kvarh, and the minimal DTR loading in peak, 110.41%, and on average, 38.84%.

Fig. 20 shows the daily behaviour of the secondary criteria for the urban grid with no-control and with different control strategies for a DTR primary voltage of 0.96 p.u. The *Q*-exchange is shown in Fig. 20(a); the DTR loading in Fig. 20(b) and the loss in Fig. 20(c). Simulation results show that cos*φ*(*P*)-control provokes the maximal peak values for all secondary criteria as follows: $\widehat{Q}^{ex}$ = 482.47 kvar; $\widehat{\text{DTRL}}$ = 143.28% and $\widehat{P}^{loss}$ = 60.35 kW. Furthermore, it provokes the maximal reactive energy exchange and energy loss of 2847.67 kvarh and 285.04 kWh, respectively, and therefore also the maximal average DTR loading of 46.09%. The minimal peak and energy loss of 39.47 kW and 205.77 kWh, respectively, is provoked by *L*(*U*)-control combined with *Q*-Autarkic prosumers. This combination also provokes the minimal *Q*-exchange in peak, 11.68 kvar, and in total, 51.57 kvarh, and the minimal DTR loading in peak, 116.23%, and on average, 40.63%.

Real rural grid – Fig. 21 shows the voltage profiles of all feeders of the rural grid with no-control for maximal and minimal voltage conditions. For maximal voltage conditions, all profiles lie within and above the upper part of the allowed voltage range; two feeders violate the upper voltage limit, resulting in a peak voltage violation index of 1.566 and 0.169 for a DTR primary voltage of 1.06 p.u. and 1.01 p.u., respectively. The calculation over the 24 h time horizon yields an average voltage violation index (primary criterion) of 0.259 and 0.015 for a DTR primary voltage of 1.06 p.u. and 1.01 p.u., respectively. For minimal voltage conditions, the profile stays within the lower part of the allowed voltage range throughout the whole day. Fig. 22 shows the voltage profiles of all feeders of the urban grid for maximal voltage conditions and different control strategies. They are shown for cos*φ*(*P*)-, *Q*(*U*)-, *L*(*U*)- and *L*(*U*)-control combined with *Q*-Autarkic prosumers in

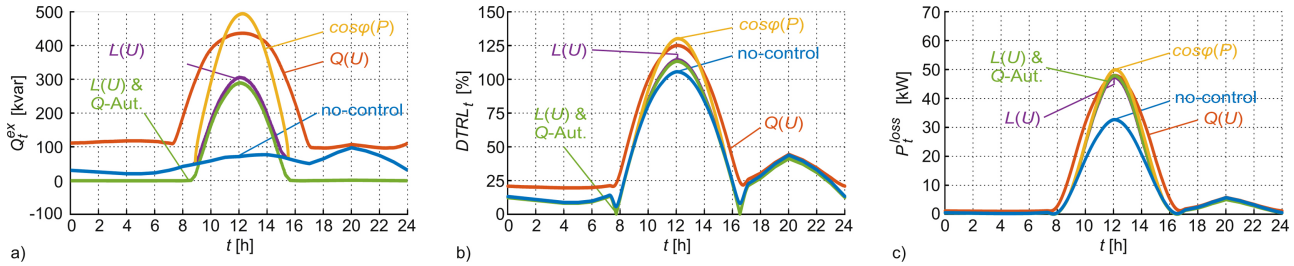

Fig. 18. Daily behaviour of the secondary criteria for the urban grid with no-control and with different control strategies for a maximum DTR primary voltage of 1.06 p.u.: (a) *Q*-exchange; (b) DTR loading; (c) active power loss.

Figs. 22(a)–(d). For a DTR primary voltage of 1.06 p.u., cosφ(*P*)- and *Q*(*U*)-control do not eliminate all violations of the upper voltage limit, resulting in a peak voltage violation index of 0.074 and 0.053, respectively. The calculation over the 24 h time horizon yields an average voltage violation index (primary criterion) of 0.011 and 0.002, respectively, for these control strategies. For a DTR primary voltage of 1.01 p.u. and 0.96 p.u., all control strategies eliminate the violations of the upper voltage limit throughout the whole day.

Figs. 23–25 show the daily behaviour of the secondary criteria for the rural grid with no-control and with different control strategies for different DTR primary voltages of 1.06, 1.01 and 0.96 p.u., respectively. For all DTR primary voltages, if no-control is exercised, the *Q*-exchange is determined exclusively by the prosumers' consumption and thus follows the load profile shown in Fig. 4, while the DTR loading and grid loss are determined by their consumption and PV-production. Consequently, if no-control is exercised, the peak *Q*-exchange occurs at around 8 p.m. for all DTR primary voltages. Results show that *L*(*U*)-control, if combined with *Q*-Autarkic prosumers, and cosφ(*P*)-control, are active only during PV-production periods for all DTR primary voltages. For a maximum DTR primary voltage of 1.06 p.u., *Q*(*U*)-control is active throughout the whole day; for a medium DTR primary voltage of 1.01 p.u., it is active only during PV-production and low load (between midnight and 7 a.m.) periods; and for a minimum DTR primary voltage of 0.96 p.u., it is active only during PV-production and high load (at around 8 p.m.) periods. *L*(*U*)-control, if not combined with *Q*-Autarkic prosumers, is active only during PV-production periods for DTR primary voltages of 1.06 and 1.01 p.u., but for lower DTR primary voltages, e.g. 0.96 p.u., it is inactive throughout the whole day. cosφ(*P*)-, *Q*(*U*)- and *L*(*U*)-control combined with *Q*-Autarkic prosumers provoke the peak *Q*-exchange at around 12 p.m. for all DTR primary voltages. If *L*(*U*)-control is not combined with *Q*-Autarkic prosumers, it provokes the peak *Q*-exchange at around 12 p.m. for DTR primary voltages of 1.06 and 1.01 p.u., respectively, and at around 8 p.m., for a DTR primary voltage of 0.96 p.u.

Fig. 23 shows the daily behaviour of the secondary criteria for the rural grid with no-control and with different control strategies for a DTR primary voltage of 1.06 p.u. The *Q*-exchange is shown in Fig. 23(a); the DTR loading in Fig. 23(b) and the loss in Fig. 23(c). Simulation results show that *Q*(*U*)-control provokes the maximal peak *Q*-exchange, reactive energy exchange, peak and average DTR loading and energy loss as follows: $\widehat{Q}^{\mathrm{ex}} = 177.74$ kvar; $E^{Q_{\mathrm{ex}}} = 2835.75$ kvarh; $\widehat{\mathrm{DTRL}} = 181.91\%$; $\overline{\mathrm{DTRL}} = 91.35\%$ and $E^{P_{\mathrm{loss}}} = 172.55$ kWh. Meanwhile, *L*(*U*)-control combined with *Q*-Autarkic prosumers provokes the maximal peak loss of 25.83 kW, the minimal *Q*-exchange in peak, 108.33 kvar, and in total, 534.39 kvarh, and the minimal DTR loading in peak, 156.24%, and on average, 52.41%. The minimal peak and energy loss of 24.14 kW and 113.39 kWh, respectively, is provoked by cosφ(*P*)-control.

Fig. 24 shows the daily behaviour of the secondary criteria for the rural grid with no-control and with different control strategies for a DTR primary voltage of 1.01 p.u. The *Q*-exchange is shown in Fig. 24(a); the DTR loading in Fig. 24(b) and the loss in Fig. 24(c). Simulation results show that cosφ(*P*)-control provokes the maximal peak values for all secondary criteria as follows: $\widehat{Q}^{\mathrm{ex}} = 175.96$ kvar; $\widehat{\mathrm{DTRL}} = 190.81\%$ and $\widehat{P}^{\mathrm{loss}} = 26.51$ kW; furthermore, it provokes the maximal average DTR loading of 60.15%. Meanwhile, *Q*(*U*)-control provokes the maximal reactive energy exchange and energy loss of 1056.41 kvarh and 125.78 kWh, respectively. The minimal peak loss of 19.17 kW is provoked by *L*(*U*)-control, while its combination with *Q*-Autarkic prosumers provokes the minimal *Q*-exchange in peak, 45.71 kvar, and in total, 162.64 kvarh, the minimal DTR loading in peak, 154.15%, and on average, 52.56% and the minimal energy loss of

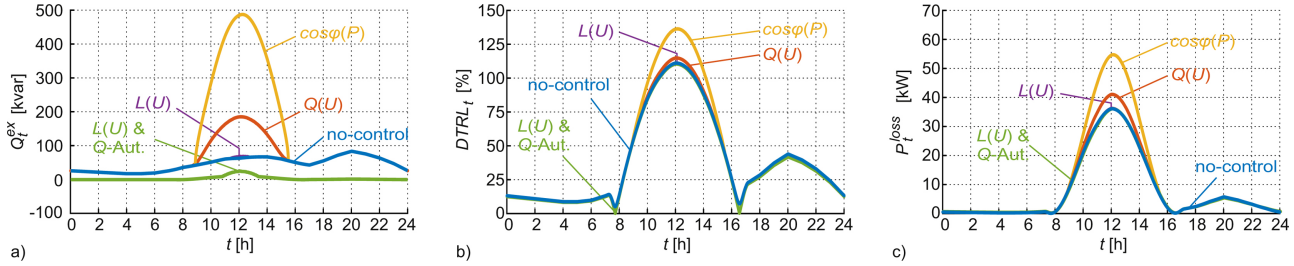

Fig. 19. Daily behaviour of the secondary criteria for the urban grid with no-control and with different control strategies for a medium DTR primary voltage of 1.01 p.u.: (a) *Q*-exchange; (b) DTR loading; (c) active power loss.

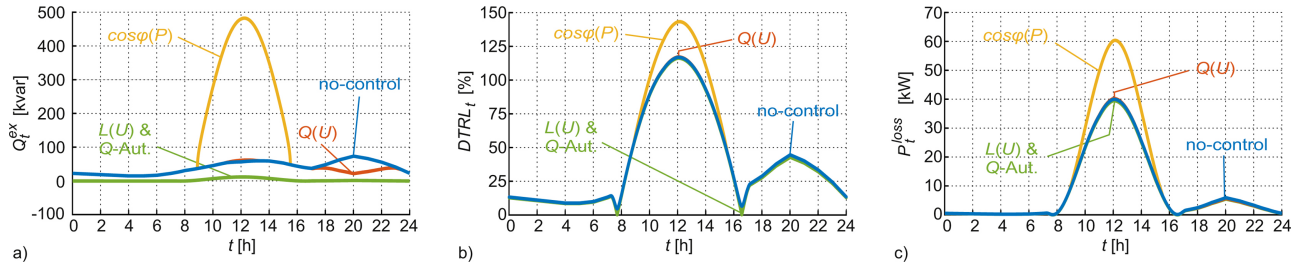

Fig. 20. Daily behaviour of the secondary criteria for the urban grid with no-control and with different control strategies for a minimum DTR primary voltage of 0.96 p.u.: (a) *Q*-exchange; (b) DTR loading; (c) active power loss.

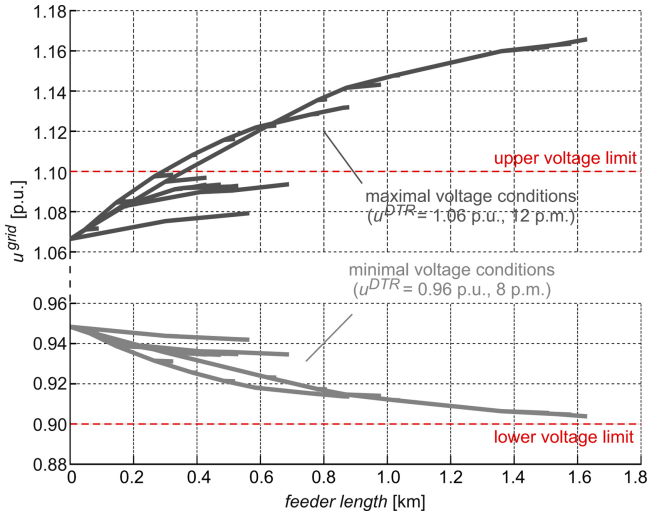

Fig. 21. Voltage profiles of all feeders of the rural grid with no-control for maximal and minimal voltage conditions.

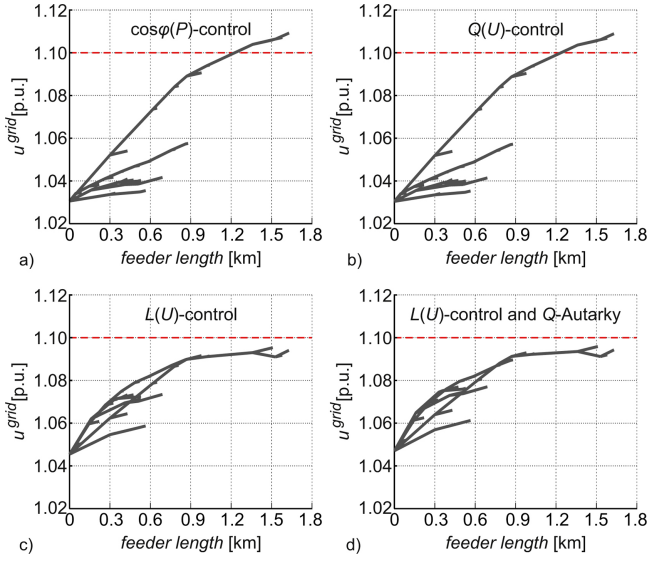

Fig. 22. Voltage profiles of all feeders of the rural grid for maximum voltage conditions and different control strategies: (a) cos*φ*(*P*); (b) *Q*(*U*); (c) *L*(*U*); (d) *L*(*U*) combined with *Q*-Autarkic prosumers.

93.22 kWh. Fig. 25 shows the daily behaviour of the secondary criteria for the rural grid with no-control and with different control strategies for a DTR primary voltage of 0.96 p.u. The *Q*-exchange is shown in Fig. 25(a); the DTR loading in Fig. 25(b) and the loss in Fig. 25(c). Simulation results show that cos*φ*(*P*)-control provokes the maximal peak values for all secondary criteria as follows: $\widehat{Q}^{ex} = 175.49$ kvar; $\widehat{DTRL} = 200.88\%$ and $\widehat{P}^{loss} = 29.31$ kW. Furthermore, it provokes the maximal reactive energy exchange and energy loss of 1003.32 kvarh and 135.96 kWh, respectively, and therefore also the maximal average DTR loading of 62.68%. The minimal peak and energy loss of 18.31 kW and 94.97 kWh, respectively, is provoked by *L*(*U*)-control combined with *Q*-Autarkic prosumers. This combination also provokes the minimal *Q*-exchange in peak, 9.39 kvar, and in total, 45.74 kvarh, and the minimal DTR loading in peak, 159.45%, and on average, 54.63%.

5.2. Social criteria

The discrimination criterion is evaluated for *Q*-Autarky and the different local control strategies mentioned in Section 2.3. However, a coordination of these local controls reduces switching events of traditional voltage regulators, electric losses, peak demand and energy consumption, while keeping the voltages within the limits [11,16,17]. The data privacy criterion is discussed in the context of a coordination of the local controls.

5.2.1. Discrimination

In general, the reactive power demand of a prosumer plant is composed of its internal loads' and PV-inverter's *Q*-consumption. This composition is shown for the different control strategies, i.e. inverter- and inductive device Volt/var control and *Q*-Autarky, in Table 4. In case of an inverter Volt/var control, the prosumer plants draw reactive power from the LVG to cover the reactive power needs of their loads, and to contribute to voltage control in LVG. Also in case of an inductive device Volt/var control, the loads receive the needed reactive power from the LVG, but no other reactive power exchange between prosumer and LVG is necessary. *Q*-Autarkic prosumers cover their reactive power demand locally, thus no reactive power exchange is required.

In case of an inverter Volt/var control, the PV-inverters provide reactive power for voltage control in LVG. With the assumption of equal PV-production conditions (irradiance, temperature, tilt angle of PV-modules, etc.) in one LVG, all prosumers produce the same normalized active power ($p_i^{PV} = p^{PV}$). Meanwhile, the grid-voltage varies along the feeder where the PV-inverters are connected. If one common cos*φ*(*P*)- or *Q*(*U*)-characteristic is applied for all inverters within one LVG, their normalized reactive power contribution ($q_i^{inv} = Q_i^{inv}/S_r^{inv}$) can be expressed by Eqs. (25) and (26), respectively.

$$q_i^{inv} = f^{\cos\varphi(P)}(p^{PV}) \tag{25}$$

$$q_i^{inv} = f^{Q(U)}(U_i^{grid}) \tag{26}$$

where:

$f^{\cos\varphi(P)}$ – relation between q_i^{inv} and p^{PV};

$f^{Q(U)}$ – relation between q_i^{inv} and U_i^{grid}.

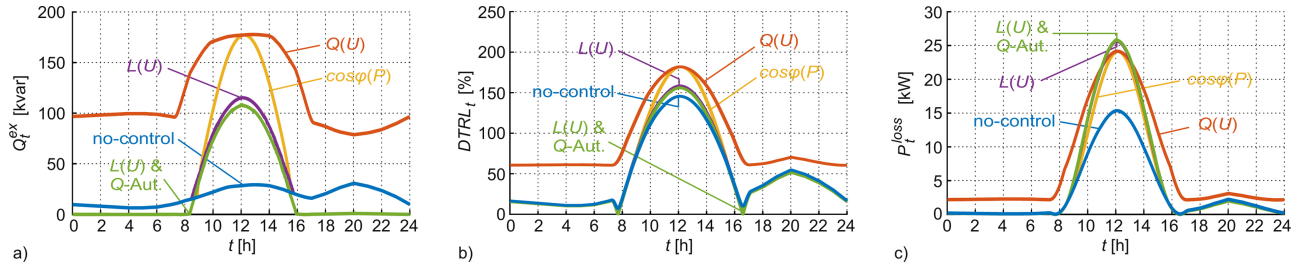

Fig. 23. Daily behaviour of the secondary criteria for the rural grid with no-control and with different control strategies for a maximum DTR primary voltage of 1.06 p.u.: (a) *Q*-exchange; (b) DTR loading; (c) active power loss.

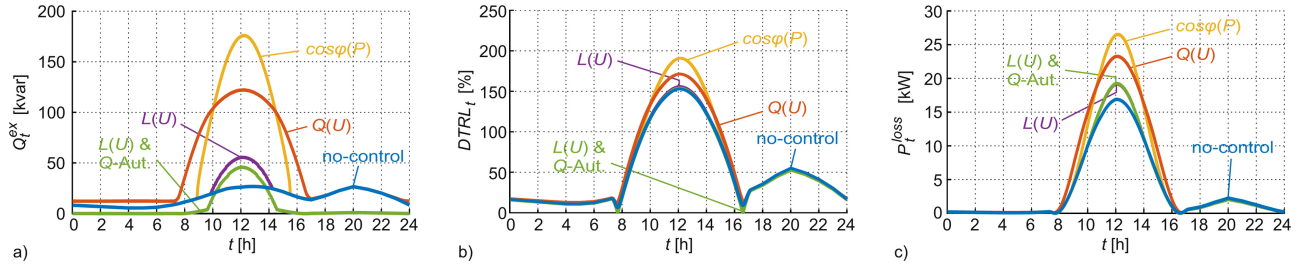

Fig. 24. Daily behaviour of the secondary criteria for the rural grid with no-control and with different control strategies for a medium DTR primary voltage of 1.01 p.u.: (a) *Q*-exchange; (b) DTR loading; (c) active power loss.

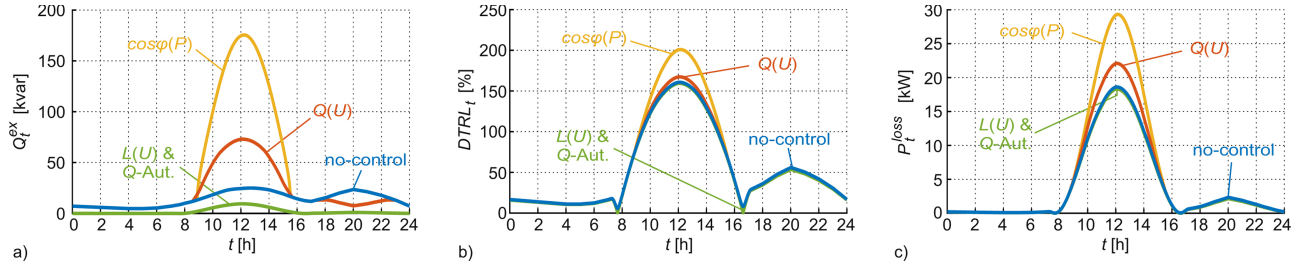

Fig. 25. Daily behaviour of the secondary criteria for the rural grid with no-control and with different control strategies for a minimum DTR primary voltage of 0.96 p.u.: (a) *Q*-exchange; (b) DTR loading; (c) active power loss.

Table 4
Q-capabilities of prosumer *i* for different control strategies.

Ctrl. strategy	Inverter	Load	Prosumer
Inverter ctrl.	Q_i^{inv}	Q_i^{load}	$Q_i^{\text{inv}} - Q_i^{\text{load}}$
Ind. device ctrl.	0	Q_i^{load}	Q_i^{load}
Q-Autarky	Q_i^{load}	Q_i^{load}	0

Eq. (25) shows that all cos*φ*(*P*)-controlled inverters provide the same amount of normalized reactive power. In contrast, every *Q*(*U*)-controlled one provides a different amount of it, Eq. (26). Consequently, prosumers using cos*φ*(*P*)-control are not discriminated, but in case of local *Q*(*U*)-control, a discrimination appears.

In case of an inductive device Volt/var control, whether or not combined with *Q*-Autarkic prosumers, the prosumers do not contribute to voltage control in LVG, and thus they cannot be discriminated at all.

5.2.2. Data privacy

Fig. 26 shows the data flows required to coordinate the local Volt/var controls within the LVG for three different cases. The inverters and inductive devices are connected to the centralized controller via communication gates. Fig. 26(a) shows the data exchanges between DSO and prosumers that are needed for a centralized control of the PV-inverters. Thus, data privacy is jeopardized. Meanwhile, Fig. 26(b) shows the data flows required for the centralized control of inductive devices. In this case, data are exchanged only between devices of the DSO. Data exchange between the DSO and the prosumers is not necessary. Consequently, data privacy is preserved. Fig. 26(c) shows the data flows in case of *Q*-Autarky and a centralized control of inductive devices. The implementation of *Q*-Autarky does not require any additional data exchanges between the DSO and prosumers, and thus does not impair the data privacy.

5.3. Overall evaluation

The results of the social assessment and all simulated scenarios are

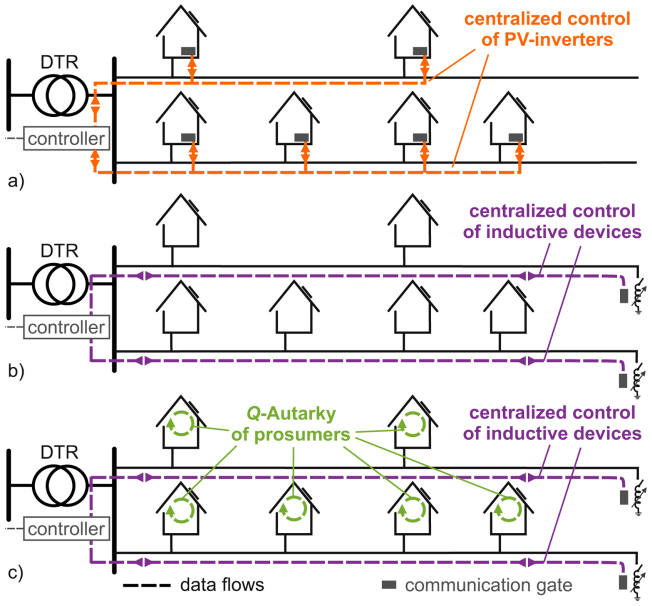

Fig. 26. Schematic LVG and the data flows required to perform different control strategies: (a) centralized control of PV-inverters; (b) centralized control of inductive devices; (c) *Q*-Autarky of prosumers and centralized control of inductive devices.

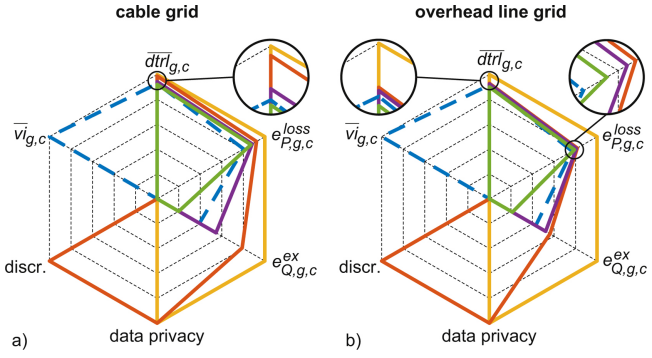

Fig. 27. Spider charts of Volt/var control strategies for different theoretical grids: (a) cable; (b) overhead line.

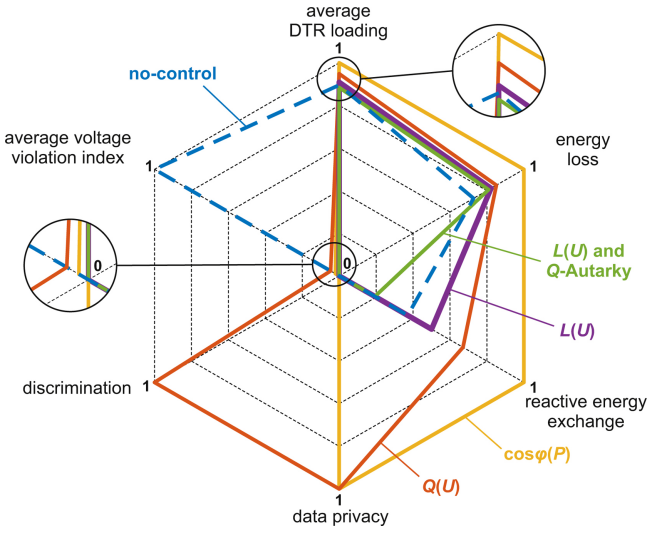

Fig. 28. Spider chart of Volt/var control strategies for the real grids.

summarized and visualized in spider charts. Results for control strategies are presented by full lines in different colors: cos$\varphi(P)$ in yellow, $Q(U)$ in orange, $L(U)$ in purple and $L(U)$ combined with Q-Autarkic prosumers in green. Meanwhile, results for no-control are marked by a dashed blue line.

5.3.1. *Theoretical grids*

Fig. 27(a) shows the spider chart of the considered Volt/var control strategies for the theoretical cable grid. In this grid, all control strategies eliminate the voltage limit violations and at the same time increase the grid loss. cos$\varphi(P)$-control provokes the highest average DTR loading, energy loss and reactive energy exchange, compared to the other control strategies. Data privacy is not guaranteed. $Q(U)$ shows smaller values for the secondary criteria, compared to cos$\varphi(P)$, but prosumers are discriminated and their data privacy is jeopardized. The use of $L(U)$ further improves the secondary criteria, compared to that of $Q(U)$. Furthermore, data privacy of prosumers is preserved and they are not discriminated. Its combination with Q-Autarkic prosumers shows the best results for all considered criteria. As a result, the surface stretched by cos$\varphi(P)$-control is the largest, while the one stretched by $L(U)$-control combined with Q-Autarkic prosumers is the smallest.

Fig. 27b) shows the spider chart of the considered Volt/var control strategies for the theoretical overhead line grid. Also in this case, the same trend is observed as in the theoretical cable grid discussed above.

As a result, the observed trend is independent from the cable share of the LVG. Therefore, results for both real grids are presented in a unique chart, Eqs. (21)–(24).

5.3.2. *Real grids*

Fig. 28 shows the assessment of the considered Q-control strategies for both real grids together. The same trend is observed for the real grids as for the theoretical ones. Also under realistic grid conditions, the surface stretched by cos$\varphi(P)$-control is the largest, while the one stretched by $L(U)$-control combined with Q-Autarkic prosumers is the smallest. Here, it has to be underlined that in rural grids with relative long feeders, neither cos$\varphi(P)$- nor $Q(U)$-control eliminate all violations of the upper voltage limit.

6. Conclusion

The investigated control strategies clearly differ from each other in terms of prosumer discrimination, violation of their data privacy, elimination of voltage limit violations, reactive power exchange between MVG and LVG, distribution transformer loading and grid loss.

Control strategies which involve prosumer-owned PV-inverters in voltage control entail social issues like prosumer discrimination and violation of their data privacy. Local $Q(U)$-control always provokes a discrimination. A coordination of local inverters Volt/var controls requires extensive data exchanges between DSO and prosumers. In contrast, the use of DSO-owned inductive devices to control the grid-voltage causes neither discrimination of prosumers nor violation of their data privacy.

Simulation results show that in low voltage grids with radial structure and high PV-penetration, cos$\varphi(P)$- and $Q(U)$-controlled inverters consume more reactive power in total than local $L(U)$-controls. This results in significantly higher reactive power exchanges, distribution transformer loadings and grid losses, in average. This trend prevails in cable and overhead line feeders, as well as in mixed ones. Both control strategies for PV-inverters are not sufficient to eliminate all voltage limit violations in rural grids. $L(U)$ does eliminate all limit violations. Its combination with Q-Autarkic prosumers further improves the technical criteria.

Finally, the cos$\varphi(P)$-control strategy shows the worst overall performance, while $L(U)$-control combined with Q-Autarkic prosumers shows the best one.

This paper is focused on the static performance of different Volt/var control strategies. However, their dynamic behaviour is a quite relevant issue that is currently subject of other ongoing works.

Appendix A

In this section is illustrated the adequacy of the $Q(U)$-parameterizations used for both real grids, urban and rural.

Fig. 29(a) shows the voltage profile of the urban grid's longest feeder for two cases: maximal PV-injection and DTR primary voltage combined with minimal load (≙ maximal voltages) and minimal PV-injection and DTR primary voltage combined with maximal load (≙ minimal voltages). Fig. 29(b) shows the $Q(U)$-characteristic used for the urban grid; the parts of the characteristic the PV-inverters cover for maximal and minimal voltages are outlined as dotted lines.

For maximal voltages, the inverters absorb almost the minimal amount of reactive power which is required to eliminate all violations of the upper voltage limit. For minimal voltages, the inverters inject some reactive power and thus partly cover the loads' Q-demands, resulting in reduced Q-flows within the LVG. For voltages between 0.94 p.u. and 1.04 p.u., the inverters do not exchange any reactive power with the LVG.

Fig. 30(a) shows the voltage profile of the rural grid's longest feeder for two cases: maximal PV-injection and DTR primary voltage combined with minimal load (≙ maximal voltages) and minimal PV-injection and DTR primary voltage combined with maximal load (≙ minimal voltages). Fig. 30(b) shows the $Q(U)$-characteristic used for the rural grid; the parts of the characteristic the PV-inverters cover for maximal and minimal voltages are outlined as dotted lines.

For maximal voltages, $Q(U)$-control is not sufficient to eliminate all violations of the upper voltage limit, even though all inverters absorb their maximum reactive power. For minimal voltages, the inverters inject some reactive power and thus partly cover the loads' Q-demands, resulting in reduced Q-flows within the LVG. For voltages between 0.93 p.u. and 1.00 p.u., the inverters do not exchange any reactive power with the LVG.

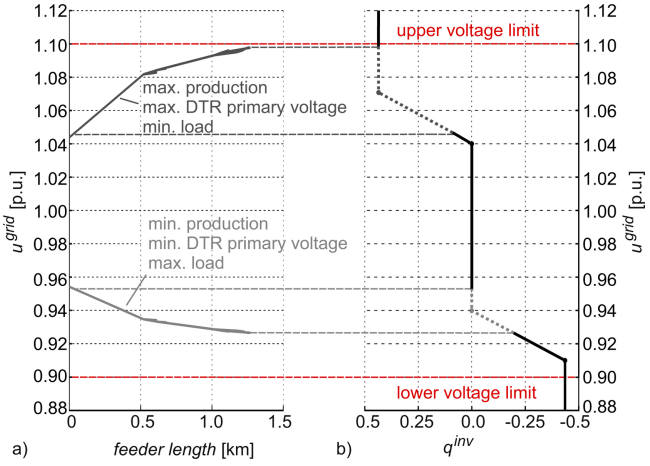

Fig. 29. Parameterization of $Q(U)$-control for the urban grid: (a) voltage profile of the longest feeder for two cases; (b) simulated $Q(U)$-characteristic.

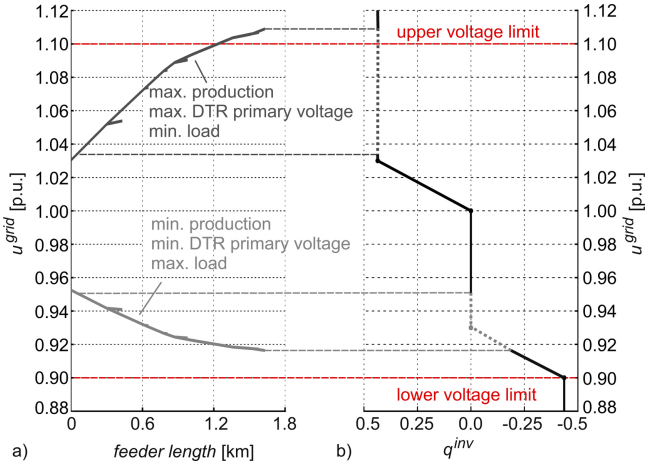

Fig. 30. Parameterization of $Q(U)$-control for the rural grid: (a) voltage profile of the longest feeder for two cases; (b) simulated $Q(U)$-characteristic.

References

[1] S. Hashemi, J. Østergaard, Methods and strategies for overvoltage prevention in low voltage distribution systems with PV, IET Renew Power Gener. 11 (2) (2017) 205–214, https://doi.org/10.1049/iet-rpg.2016.0277.

[2] O. Marggraf, S. Laudahn, B. Engel, M. Lindner, C. Aigner, R. Witzmann, M. Schoeneberger, S. Patzack, H. Vennegeerts, M. Cremer, M. Meyer, A. Schnettler, I. Berber, T. Buelo, J. Brantl, F. Wirtz, R. Frings, F. Pizzutto, U-control – analysis of distributed and automated voltage control in current and future distribution grids, International ETG Congress 2017 (2017) 1–6.

[3] IEEE Std 1547-2018 (Revision of IEEE Std 1547-2003), IEEE standard for interconnection and interoperability of distributed energy resources with associated electric power systems interfaces, (2018), pp. 1–38, https://doi.org/10.1109/IEEESTD.2018.8332112.

[4] A. Ilo, D.-L. Schultis, C. Schirmer, Low-voltage grid behavior in the presence of concentrated var-sinks: capacity release by *Q*-autarkic customers, Elsevier – Electric Power Systems Research (submitted for publication).

[5] A. Ilo, D.-L. Schultis, C. Schirmer, Effectiveness of distributed vs. concentrated volt/var local control strategies in low-voltage grids, Appl. Sci. 8 (8).

[6] F. Zhang, X. Guo, X. Chang, G. Fan, L. Chen, Q. Wang, Y. Tang, J. Dai, The reactive power voltage control strategy of PV systems in low-voltage string lines, 2017 IEEE Manchester PowerTech (2017) 1–6, https://doi.org/10.1109/PTC.2017.7980995.

[7] C. Winter, R. Schwalbe, M. Heidl, W. Prüggler, Harnessing PV inverter controls for increased hosting capacities of smart low voltage grids, in: U. Betancourt (Ed.), 4th International Workshop on Integration of Solar Power into Power Systems, Energynautics GmbH, 2014.

[8] B. Bletterie, A. Goršek, B. Uljanić, B. Blažič, A. Woyte, T.V. Van, F. Truyens, J. Jahn, Enhancement of the network hosting capacity – clearing space for/with PV, 5th World Conference on Photovoltaic Energy Conversion, Valencia, Spain, 2010.

[9] K. Turitsyn, P. Sulc, S. Backhaus, M. Chertkov, Options for control of reactive power by distributed photovoltaic generators, Proc. IEEE 99 (6) (2011) 1063–1073, https://doi.org/10.1109/JPROC.2011.2116750.

[10] A. Ilo, Effects of the reactive power injection on the grid – the rise of the volt/var interaction chain, Smart Grid Renew. Energy 7 (7) (2016) 217–232, https://doi.org/10.4236/sgre.2016.77017.

[11] M. Juamperez, G. Yang, S.B. Kjær, Voltage regulation in LV grids by coordinated volt–var control strategies, J. Modern Power Syst. Clean Energy 2 (4) (2014) 319–328, https://doi.org/10.1007/s40565-014-0072-0.

[12] D.-L. Schultis, A. Ilo, TUWien_LV_TestGrids, Mendeley, (2018), https://doi.org/10.17632/hgh8c99tnx.1 (dataset).

[13] A. Bokhari, A. Alkan, R. Dogan, M. Diaz-Aguiló, F. de León, D. Czarkowski, Z. Zabar, L. Birenbaum, A. Noel, R.E. Uosef, Experimental determination of the ZIP coefficients for modern residential, commercial, and industrial loads, IEEE Trans. Power Delivery 29 (3) (2014) 1372–1381, https://doi.org/10.1109/TPWRD.2013.2285096.

[14] E-Control, Technische und organisatorische Regeln für Betreiber und Benutzer von Netzen, Besondere technische Regeln/Parallelbetrieb von Erzeugungsanlagen mit Verteilernetzen, Teil D/Hauptabschnitt D4, 2016.

[15] Proposal for a directive of the European parliament and of the council on common rules for the internal market in electricity (recast), COM/2016/0864 final/2 – 2016/0380 (COD). URL http://eur-lex.europa.eu/legal-content/EN/ALL/?uri=CELEX:52016PC0864R(01).

[16] H. Ravindra, M.O. Faruque, K. Schoder, M. Steurer, P. Mclaren, R. Meeker, Dynamic interactions between distribution network voltage regulators for large and distributed PV plants, PES T D 2012 (2012) 1–8, https://doi.org/10.1109/TDC.2012.6281599.

[17] R. Zafar, J. Ravishankar, Coordinated control of step voltage regulator and d-statcom in the presence of distributed photovoltaic systems, 2016 IEEE International Conference on Power System Technology (POWERCON) (2016) 1–6, https://doi.org/10.1109/POWERCON.2016.7753847.